Control-oriented thermal modeling methodology for water-cooled PEM fuel cell based systems

José David Rojas, *Member, IEEE*, Cristian Kunusch *Member, IEEE*, Carlos Ocampo-Martinez *Senior Member, IEEE*, and Vicenç Puig

***Abstract*—In this paper, a new control-oriented modelling methodology for the thermal dynamics of water-cooled Proton Exchange Membrane Fuel Cells (PEMFC) is presented and validated. This methodology is not only useful for control applications, but also can be used for predicting the temperature variation across the stack, allowing to monitor its operation. The methodology has been validated in a real 600W, 20-cells, water cooled PEMFC, with encouraging results for both the stationary and the transient states. Results show that the proposed methodology is accurate and suitable for control purposes**

***Index Terms*—Fuel cells, modelling, thermal modelling, water cooling**

NOMENCLATURE

c_p	Specific heat capacity
C_{ai}	Thermal capacitance of the left aluminium
C_b	Thermal capacitance of the inner cathode and anode graphite plates
C_{bai}	Thermal capacitance of the first anode graphite plate
C_{bad}	Thermal capacitance of the last anode graphite plate
C_{ad}	Thermal capacitance of the right aluminium plate
h	convection heat transfer for the cooling channel
K_x	x-parameter for the heat exchanger
$\dot{m}$	cooling water mass flow
R_x	x-thermal resistance
$P_{m,i}$	Power generated by i-membrane
q_i	Heat drawn from the membrane to the cooling channel
Q_c	Heat removed from the cell
T_{ad}	Temperature of the right-side endplate
T_{ai}	Temperature of the left-side endplate
T_{amb}	Temperature around the stack
$T_{ba,i}$	Temperature of the graphite plate in the anode side of each i-membrane
$T_{bc,i}$	Temperature in the graphite plate of the cathode side of the i-membrane
$T_{c,in}$	Input water temperature
$T_{c,out}$	Output water temperature
$T_{cp,i}$	Temperature of the coolant plate, associated with the i-membrane
$T_{m,i}$	Temperature of the i-membrane
T_{rc}	Temperature of the heat exchanger walls
T_{woutc}	Temperature of the output water of the cooling system

J.D. Rojas is with Escuela de Ingeniería Eléctrica. Universidad de Costa Rica. Apartado Postal 11501-2060 UCR, San José, Costa Rica. email: jdrojas@eie.ucr.ac.cr

C. Kunusch, C. Ocampo-Martinez and V. Puig are with Institut de Robòtica i Informàtica Industrial (CSIC-UPC), Universitat Politècnica de Catalunya - BarcelonaTech, C/ Llorens i Artigas 4-6. 08028 Barcelona, Spain. email: {ckunusch, cocampo, vpuig}@iri.upc.edu

Corresponding author: José David Rojas, email: jdrojas@eie.ucr.ac.cr

I. INTRODUCTION

IT is widely known that fuel cells are a promissory technology to generate electric power from fuel without a combustion process [1], [2]. Even though the scientific principles behind fuel cells are known since the 19th century, it was considered more a curiosity than a viable technology for energy conversion until the mid of the 20th century with the advances in space exploration [3].

Among different types of fuel cells, the Proton Exchange Membrane Fuel Cell (PEMFC) is one of the most popular [4]. Given its low temperature operation, it is considered as a viable power source for mobile and transport applications [5], [6]. However, this low temperature of operation also implies some technical drawbacks, because it becomes necessary to use platinum as catalyst to fasten the reaction rate. In fact, the temperature management of the PEMFC has been found to be an important issue to be solve in order to contribute to the widespread adoption of fuel cells, since the system is quite sensitive to the temperature variation and the proper operation of PEMFC depends on the hydration of the membranes, which in turn, is also sensitive to the internal temperature [7], [8].

Several modelling methodologies can be found in the PEMFC literature. In [9], both the sensible and the latent heat are taken into account in some approaches to model the thermal dynamics and steady state of a Ballard PEMFC stack. In this case, only the stack temperature is computed, since the stack itself is considered as a single component, without taking into account the individual cell temperatures. In [10], a model for the coolant circuit is presented and the temperature is controlled by using fuzzy logic techniques. The thermal model presented in this paper considers the same temperature along the whole fuel cell stack while applying an energy balance to model the system without considering the spatial variation of temperature across the stack.

The regulation of temperature using coolants is treated in [11]. The coolant circuit has a water reservoir, a radiator and a bypass valve to control the stack temperature. Two different control strategies are proposed. First, a PI control is used to keep the temperature of the water reservoir constant by manipulating the bypass valve. The second loop is a PI control that varies the flow rate of the coolant depending on the stack temperature in the feedback path and the current flow in a

feedforward path. The air supply is also controlled with a feedforward function. The other strategy is a state feedback controller, designed by means of the LQR approach based on a linearised model. However, in this case neither the thermal modelling of the stack takes into account the variation in temperature, nor the proposed model for the coolant circuit takes into account the transient dynamics of the radiator and fan subsystems.

In [12], a lumped parameter dynamic model is presented based on the models by Pukrushpan [13] taking into account the modelling of the water pump for cooling and the effect over the stack temperature. However, the model parameters are determined by values found on the literature and only a simulation study is done without a validation by using a real system. In [14],a PEMFC is modelled including the temperature of the stack. In this case, the model is validated using a 1.2 W Nexa Power Module. However, the system uses air for cooling purposes rather than water (as the methodology presented here). In [15], a PEMFC model is presented in which each single cell of the stack is considered as a lumped mass, given a more complex model than in [14], but the cooling method uses also air and not water flow. In the model methodology presented in this paper, the stack is also separated in small lumped sections as in [15], nevertheless each component of the cell is also considered in order to better accomodate the effect of water cooling on the stack.

Heat transfer was also studied in [8] using finite element analysis for a configuration that includes a cooling fin in the bipolar plates. A complex 3-D nodal modelling approach has been presented and implemented in [16] using parallel computing in order to have more accurate results by dividing the stack into several nodes.

These models fall in two different categories: either they are too simple and only consider the PEMFC as a single mass with the same temperature, or they are too complex and therefore require high computational burden. The former are useful for control purposes [17] or as substitutes for real stacks in hardware-in-the-loop emulations ([18]–[20]) while the later are employed when it is necessary to have large precision for simulation [21]. Other type of modelling paradigms, in the realm of bio-inspired models, have been also considered, as for example fuzzy logic in [22] or artificial neural networks in [23].

To overcome this situation, the modelling methodology presented in this paper is a trade-off: mathematically simple but able to simulate not only time-domain dynamics but also accurate enough to characterise how the heat is distributed across the stack. It is based on a modular approach oriented to control applications but also useful to model the temperature variation of each cell within a stack considering that the stack is cooled by means of a water flow between the cells instead of air [24]. The model has been validated in a real 20-cell PEMFC, being able to predict the stationary and transient states of the plant by tuning only a reduced set of parameters.

The reminder of the paper is organised as follows: in Section II, the proposed general thermal modelling methodology is presented in a way that can be applied to any number of cells in the stack. In Section III, the methodology is validated in a real 20-cell bench station with promising results for control developments. The conclusions are drawn in Section IV.

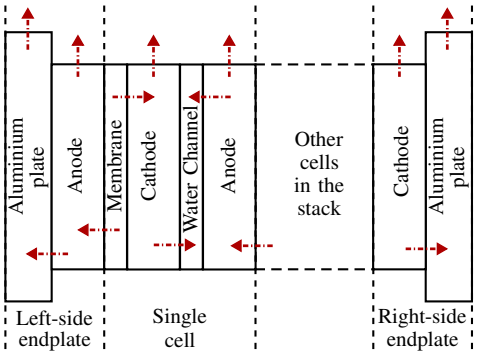

Fig. 1. Physical insight of a general system. The dashed arrows represent the considered heat flows.

II. Proposed thermal modelling methodology

A thermal modelling methodology is presented for water cooled PEM fuel cells, in order to be used in automotive applications [25]. A general thermal modelling approach for a PEMFC stack consists in following the heat flow connections between each different layer in the cell: the steel endplates, the graphite plates, the synthetic joints, the anode channels, the membrane, the gases collectors and the cathode channels. The heat flows are analysed for each section and an analogous electrical circuit is used to represent the dynamic behaviour of the system [26].

A. Modular thermal modelling

Consider the heat flows in a general water-cooled PEMFC stack as presented in Figure 1. Analysing the stack structure, the cooling circuit is placed in parallel between the anode of one cell and the cathode of the next. Therefore, the temperature of the water at the input of each cell is the same as the inlet water temperature of the stack. The average of the outlet water temperatures of all cells is used as an approximation for the outlet water temperature. The dissipated heat depends on the voltage, the theoretical maximum voltage of the fuel cell (based on the heating value of the hydrogen) and the stack current. It is assumed that this heating value remains constant for all the operation points and temperatures. The water mass flow of the coolant circuit is considered to be equally distributed along each cell inside the stack.

The heat flow from the wall of the cooling channel to the fluid is principally driven by conduction, since there is a viscous layer close to the wall, where the gradient of temperature is greater than in the rest of the fluid [27]. Then, the average temperature of the fluid would be lower than the value of this viscous layer. Considering this fact, the heat flow from the solid to the fluid is given by

$$Q = hA(T_w - T_{av}), \tag{1}$$

where h is the convection heat transfer coefficient in W/(m^{2}K), A is the effective contact area in m^2, T_{av} is the average temperature of the fluid in K, and T_w is the temperature of the

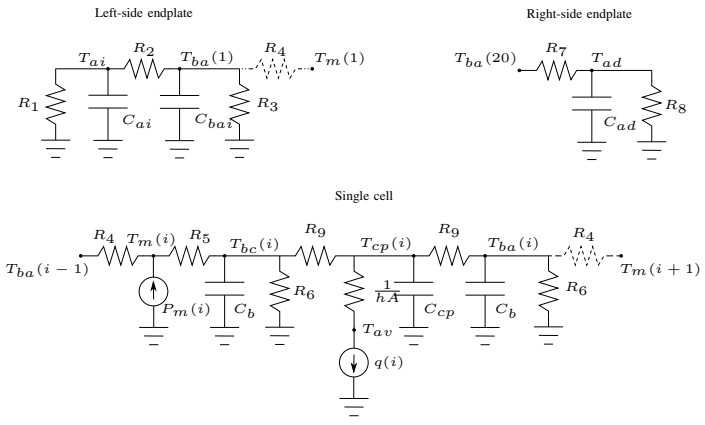

Fig. 2. Submodels of the complete PEMFC.

wall in contact with the fluid in K. The coefficient h depends on the Nusselt number[1], the geometry of the channels and the flow characteristics.

This heat in the fuel cell is removed by the circulating water, producing a temperature gradient between the input and the output of the coolant line, that is given by

$$Q_c = \dot{m}\, c_p \left(T_{c,out} - T_{c,in}\right), \tag{2}$$

where Q_c is the heat removed from the cell, $\dot{m}$ is the water mass flow trough the cell in kg/s, c_p is the specific heat capacity of the water in K/J and $T_{c,out}$ and $T_{c,in}$ are the output and input water temperature in K, respectively. For each single cell i, (1) and (2) are computed to estimate the heat drawn from the cell. As it can be seen in (1) and (2), the terms $1/(hA)$ and $1/(\dot{m}c_p)$ may be considered as thermal resistances. This fact motivates representing the thermic model directly by means of an equivalent electric circuit.

In order to be able to model a stack with an arbitrary number of cells, it is necessary to divide the complete stack in three subsystems: the left-side endplate, a single cell and the right-side endplate. The *left-side plate* takes into account the thermal capacity of the aluminium (or any other endplate material) left-side plate and the first thermal capacity of the graphite plate. The *single cell* submodel considers the heat generated by the exothermic cathode reaction, as well as the water cooling effects. Then, this subsystem is repeated p times, where p is the number of cell in the stack. If the thermal capacitance is considered as an analogous of the electrical one and the contact area between each element is considered as an electrical resistance equivalent to the thermal resistance, the model of these three subsystems can be depicted as in Fig. 2.

It has to be noticed that the polymeric membrane is considered to have a negligible thermal capacitance given that its mass is smaller than the mass of the bipolar plates in both the anode and cathode sides. The power generated by each cell is modelled as a current source, the water cooling channel is modelled as a thermal resistance and the dissipation as another current source that takes the energy out of the cell. Considering again Fig. 2, the complete model for the stack is given as follows:

[1]Ratio between the convection heat transfer for a fluid in motion and the conduction heat transfer for a motionless layer of fluid [3].

- For the left-side endplate

$$\frac{dT_{ai}}{dt} = \frac{1}{C_{ai}}\left[-\left(\frac{1}{R_1}+\frac{1}{R_2}\right)T_{ai} + \frac{1}{R_2}T_{ba1} + \frac{1}{R_1}T_{amb}\right], \tag{3}$$

$$\frac{dT_{ba,1}}{dt} = \frac{1}{C_{ba,i}}\left[-\left(\frac{1}{R_2}+\frac{1}{R_3}+\frac{1}{R_4}\right)T_{ba,1} + \frac{1}{R_2}T_{ai} + \frac{1}{R_4}T_{m,1} + \frac{1}{R_3}T_{amb}\right]. \tag{4}$$

- The generic differential equations for the single cell are given by (for $i = 1, 2, \ldots, p$):

$$\frac{dT_{bc,i}}{dt} = \frac{1}{C_b}\left[-\left(\frac{1}{R_5}+\frac{1}{R_6}+\frac{1}{R_9}\right)T_{bc,i} + \frac{1}{R_5}T_{m,i} + \frac{1}{R_9}T_{cp,i} + \frac{1}{R_6}T_{amb}\right], \tag{5}$$

$$\frac{dT_{ba,i}}{dt} = \frac{1}{C_b}\left[-\left(\frac{1}{R_4}+\frac{1}{R_6}+\frac{1}{R_9}\right)T_{ba,i} + \frac{1}{R_4}T_{m,i+1} + \frac{1}{R_9}T_{cp,i} + \frac{1}{R_6}T_{amb}\right], \tag{6}$$

$$\frac{dT_{cp,i}}{dt} = \frac{1}{C_{cp}}\left[-\left(\frac{2}{R_9}\right)T_{cp,i} + \frac{1}{R_9}T_{bc,i} + \frac{1}{R_9}T_{ba,i} - q_i\right], \tag{7}$$

and the following complementary algebraic equations:

$$T_{m,i} = \frac{R_5}{R_4+R_5}T_{ba,i-1} + \frac{R_4}{R_4+R_5}T_{bc,i} + \frac{R_4R_5}{R_4+R_5}P_{m,i}, \tag{8}$$

$$T_{cout,i} = \frac{2hA}{hA+2\dot{m}_i c_p}T_{cp,i} + \frac{2\dot{m}_i c_p - hA}{hA+2\dot{m}_i c_p}T_{cin}, \tag{9}$$

$$q_i = \frac{2hA\dot{m}_i c_p}{hA+2\dot{m}_i c_p}\left(T_{cp,i} - T_{cin}\right), \tag{10}$$

$$P_{m,i} = (1.254 - v_{c,i})\, I, \tag{11}$$

where $v_{c,i}$ is the voltage of the i-cell, I is the current drawn from the stack and m_i is the water mass flow for the i-single cell.

- For the case of the contact between the membranes and the left and right sides, (6) and (8) should be changed i.e.,

$$\frac{dT_{ba,p}}{dt} = \frac{1}{C_{bai}}\left[-\left(\frac{1}{R_6}+\frac{1}{R_7}+\frac{1}{R_9}\right)T_{ba,p} + \frac{1}{R_7}T_{ad} + \frac{1}{R_9}T_{cp,p} + \frac{1}{R_6}T_{amb}\right]. \tag{12}$$

$$T_{m,1} = \frac{R_5}{R_4+R_5}T_{ba,1} + \frac{R_4}{R_4+R_5}T_{bc,1} + \frac{R_4R_5}{R_4+R_5}P_{m,1}, \quad (13)$$

- The right-side of the stack is modelled by

$$\frac{dT_{ad}}{dt} = \frac{1}{C_{ad}}\left[-\left(\frac{1}{R_7}+\frac{1}{R_8}\right)T_{ad} + \frac{1}{R_7}T_{ba,p} + \frac{1}{R_8}T_{amb}\right], \quad (14)$$

Each parameter of the model is given as follows:

- R_1 to R_9, are the respective equivalent thermal resistance between the left aluminium end plate and the ambient; the aluminium end plate and the graphite plate of the anode; the graphite plate of the anode and the ambient; the graphite plate of the anode and the membrane; the membrane and the graphite plate of the cathode; the graphite plate of the cathode and the ambient; the graphite plate of the cathode and right aluminium plate; the right aluminium plate and the ambient; and the graphite plates and the cooling plate, respectively.
- C_{ai}, C_{bai}, C_b, C_{bad} and C_{ad} are respectively the thermal capacitance of the left aluminium end plate; the first anode graphite plate; the inner cathode and anode graphite plates; the last anode graphite plate and the right aluminium plate, respectively.
- The expression $\frac{1}{hA}$ is the equivalent thermal resistance between the cathode and the cooling fluid. h is the heat transfer coefficient ($\mathrm{W}/(\mathrm{m}^2\,^\circ\mathrm{C})$) and A is the effective area of the water channel.
- The expression $\frac{1}{\dot{m}_i c_p}$ is the equivalent thermal resistance associated with the heat removed from the fluid in the i-single cell.
- T_{amb} is the temperature around the stack, T_{cin} is the temperature of the coolant at the input, T_{cout} is the temperature of the coolant at the output, T_{cp} is the temperature of the coolant plate, T_{bc} is the temperature in the graphite plate of the cathode side of the membrane and T_{ba} is the temperature of the graphite plate in the anode side of each membrane and finally T_m is the temperature of the membrane.
- $P_m(i)$ $i \in \{1,\ldots,p\}$, is the power dissipated as heat by the electrochemical reaction for each membrane.

B. Parameter setting

As it can be seen from Section II-A, the number of parameters of the proposed model is relevant. In order to simplify the parameters setting, an implicit supposition is made: all cells in the stack can be modelled by exactly the same single cell model proposed in Fig. 2. Otherwise, the number of parameters will increase in an arithmetic progression depending on the number of cells within the stack.

The proposed procedure for parameter setting has two steps:

1) Steady state
   a) Collect data from at least ten different operating points using the following steps:
      - By means of a controller, keep the inlet-water temperature constant. It is necessary to keep the difference between the inlet-water and outlet-water temperatures below a certain threshold to avoid undesirable condensation in the gas channels.
      - Using an appropriate hydrogen and air flow rate, vary the power drawn from the stack until a new steady state is reached.
      - Write down all available temperature measurements.
   b) Initialise the values of the thermal resistances to a known value (see, e.g., [28]).
   c) If all the temperatures can be measured, from (3) to (14) it is possible to form a system of equations to perform a least square regression in order to find the values of all thermal resistances. Otherwise, an heuristic methodology has to be applied [29].
2) Transient state
   a) Initialise the values of the thermal capacitances to a known value (see, e.g., [28]).
   b) Given an operating point (for example the nominal temperature of stack operation), perform a step change first for the inlet-water temperature and second in the power drawn from the stack.
   c) Each temperature is associated to a thermal capacitance. Using only the measurement of a single cell and both endplates, manually match the response velocity of each temperature by varying the corresponding thermal capacitance according to the results given by simulations.
   d) If some temperatures are not available, change all the capacitances in the same proportion to match the velocity of all measured temperatures and compare with a simulation using the actual parameters.

III. Experimental validation

A. Description of the test bench

In this section, the modelling methodology is applied to a real 20-cell PEMFC-based bench station, shown in Fig. 3. The stack is a 600 W PEMFC, model BZ100 manufactured by UBzM. It has 20 cells with 100 cm^2 of active area and the open-circuit voltage is approximately $0.95\,\mathrm{V_{DC}}$/cell. The maximum current is 50 A at a nominal operating voltage of 12 V. The fuel-cell stack is cooled by using demineralized water through inner channels connected in parallel between each cell. The hydrogen pipeline has two normally-closed electro-valves that allow the user to select either the hydrogen for normal operation or nitrogen to purge the remaining gases. The hydrogen line also contains a gas filter, a mass-flow controller with maximum flow[2] of 30 ln/min, an anti-return check valve and a pressure transducer at the stack input. The pipeline is made of stainless steel of 1/2 inch diameter. The air line has also a gas filter, a mass-flow controller with maximum

[2]The unit ln/min are litres per minute measured at 0.00°C, 1.013 bar.

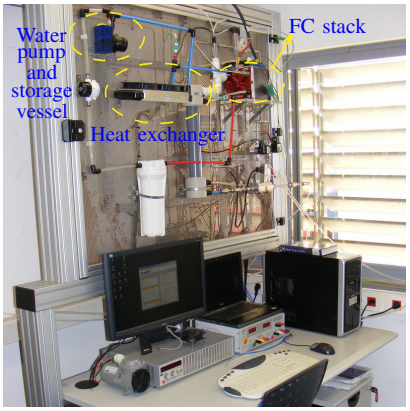

Fig. 3. PEMFC station at IRI (CSIC-UPC).

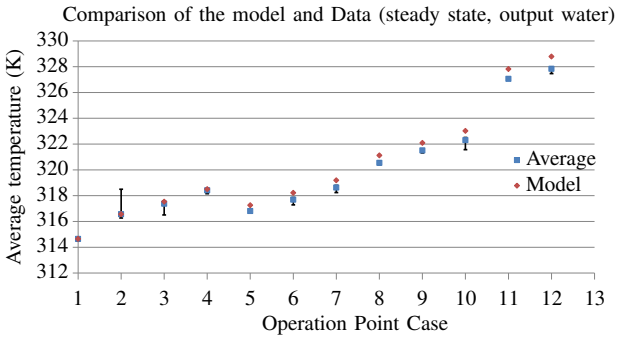

Fig. 5. Comparison of the average plant measurements and the model results in steady state case. The black bars represent the complete span of the data for each operation point.

flow rate of 150 ln/min, an anti-return check valve and a pressure transducer (0-1 bar). The cooling system is composed by a waterflow meter, a storage vessel, an electric pump and a heat exchanger with two fans for forced convection. It has also temperature transducers in both the inlet and the outlet of the PEMFC.

B. Application of the modelling methodology

The fuel-cell stack of the station has 20 cells in series, which means that the section of the model that accounts for each single cell submodel has to be replicated 20 times. The right-side plate model is similar to the left-side plate. In Fig. 2, the diagram of the each submodel is presented. This methodology leads to a system model with 63 state variables and 80 auxiliary algebraic equations (for each $T_{m,i}$, $T_{cout,i}$, q_i and $P_{m,i}$, see (8)-(11)).

Several experiments have been performed in order to validate the thermal model on the PEMFC of the test station. First, the steady state case is considered and the model parameters are computed at an operating point of 25 A with a water inlet temperature of 38°C (311.15 K). An additional set of 11 steady states cases are used for cross-validation. Secondly, the values of the thermal capacitances are determined empirically in order to derive the model dynamics.

The values of the thermal resistances R_1 to R_8 are assumed to be equal to $R_1 = R_8 = 4.2721$, $R_2 = R_7 = 0.2521$, $R_3 = R_6 = 21.0227$, $R_4 = R_5 = 0.3178$ (all in K/W). These values were obtained based on the characteristics of the materials that are common to a large set of commercial fuel-cell stacks [28]. In order to fit the parameters and validate the model, several operating points are defined (different load currents and temperatures of operation) as pointed out in Section II-B.

Despite the fact that several temperature measurements are available on the stack, these measurements are not completely useful to accurately approximate the internal temperature of the anode, membrane or cathode since the temperature sensor are superficial to the stack. Thus both water inlet and outlet temperatures are used to validate the model. In Fig. 4, the experimental data is depicted. From these data, the average value of the input and output temperatures can be obtained and analysed after the transient state is elapsed.

The values of the thermal resistance $\frac{1}{hA}$ were found based on the measurements of Case 1 in Table I, to match the outlet water temperature of the model with the average measurements from the plant. When the model has been validated with the transient state, the final parameter values are readjusted and the steady state case is revisited. The final comparison between the model and the real measurements is presented in both Table I and Fig. 5.

The maximum error is less than 0.14%, for Case 1. In Fig. 5, black bars represent the deviation of the real measurements from the average value. To maintain the value of the inlet water temperature constant (for experimental purposes only), a PI controller was first implemented to control the velocity of the fans in the cooling circuit. The water flow is kept constant in all cases. During the experiment, the ambient temperature had an increment due to the heat disspated by the stack. The difference between the maximum and minimum ambient temperature during the experiment was 2.36 K. Nevertheless, for validation purposes, it was considered to be constant at 300 K, which was the average boundary temperature of the stack during the tests.

From Fig. 5, once the values of thermal resistances and capacitances have been computed, the model is able to reproduce the behaviour of the outlet water temperature with a suitable error with respect to the average value of the measurements, in a wide range of operating points. The model dynamics depend on the values of the thermal capacitances and the thermal resistances previously obtained and outlined in Table II. Starting from the steady state of Case 1 in Table I, the electric load is changed and the temperature of the inlet water is kept constant.

After setting the value of $C_b = 26.977$ J/K and $C_{cp} = 0.2698$ J/K, the model response to a step change in the current load is presented in Fig. 6. As it can be seen in this figure, the model captures the main time constant of the plant and is able to accurately reproduce the dynamic behaviour of the system.

Other validation tests have been performed at different operating points, confirming the model accuracy and reliability. As an example, the heating process of the stack is presented, from room temperature to approximately 318.15 K. The load varies from 0 W to 456 W in approximately 30 min in discrete

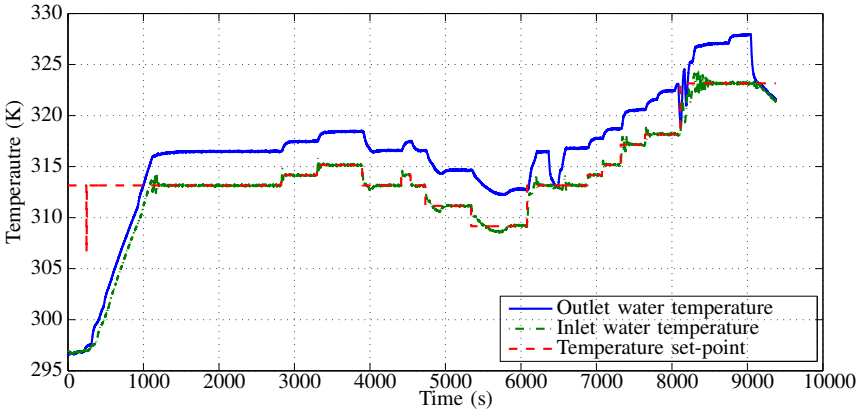

Fig. 4. Typical experiment to fit and validate the model in steady state.

TABLE I
OPERATING POINT CASES

Case	Load Current (A)	Average Inlet Water Temp. (K)	Average Cell Voltage (V)	Average Outlet Water Temp. (K)	Model Outlet Water Temp (K)	Difference (%)
1	**25**	**311.15**	**0.66**	**314.65**	**314.21**	**-0.14**
2		313.15	0.67	316.56	316.16	-0.13
3		314.15	0.67	317.37	317.13	-0.08
4		315.15	0.67	318.41	318.11	-0.10
5	30	313.15	0.68	316.81	316.70	-0.03
6		314.15	0.68	317.69	317.67	-0.01
7		315.15	0.68	318.63	318.66	0.01
8		317.15	0.68	320.54	320.60	0.02
9		318.15	0.68	321.51	321.57	0.02
10	35	318.15	0.66	322.31	322.39	0.03
11		323.15	0.67	327.06	327.20	0.04
12	40	323.15	0.64	327.84	328.05	0.07

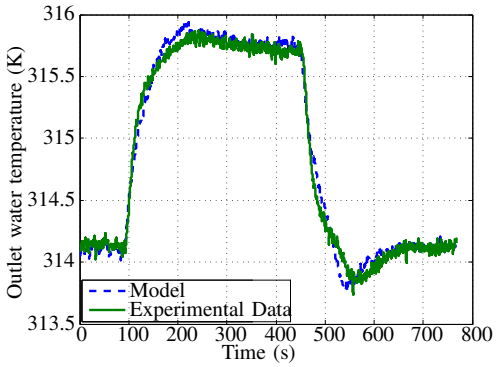

Fig. 6. Transient response of the model after empirically finding the values of the thermal capacitances.

steps. The inlet water temperature set-point is 315.15 K. The variation of the stack voltage is presented in Fig. 7b and the variation of the stack current is presented in Fig. 7a.

In this test, a typical start-up behaviour of the stack is considered. At the beginning of the experiment, the flow of hydrogen in the stack was null. Once the stack is fed with hydrogen, the voltage reaches approximately 17.5 V quickly, and when the current is set to 5 A, the voltage falls to 15 V (approximately 0.75 V/cell). At $t = 1000$ s, the inlet water temperature reaches the set-point and the PI controller that regulates the inlet water temperature is activated. The variation of the inlet water temperature is presented in Fig. 7c. The load was disconnected at time $t = 1190$ s and $t = 1490$ s.

Regarding the initial condition of the model, all the different states are set to 300 K (room temperature). The comparison between the outlet water temperature between the model and the real data is presented in Fig. 7d. Notice that the model is able to follow the variation of the outlet water temperature accurately during the entire experiment. The difference at the beginning of the experiment is caused by the difference between the initial conditions of the model and the real internal temperatures of the stack. The average of the absolute value of the error is less than 0.4955 K. Part of the error is because certain thermal inertia that is found when a sudden change in the inlet water temperature appears. To overcome this problem, an option is to add a thermal capacitance for the outlet water temperature. But this change represents 20 more states if the model presented in Section II-A is changed. Given that the output error in the model is small, this change is not considered, but it could be addressed as an improvement for applications that require a more accurate representation.

The experiments show that the model is able to represent

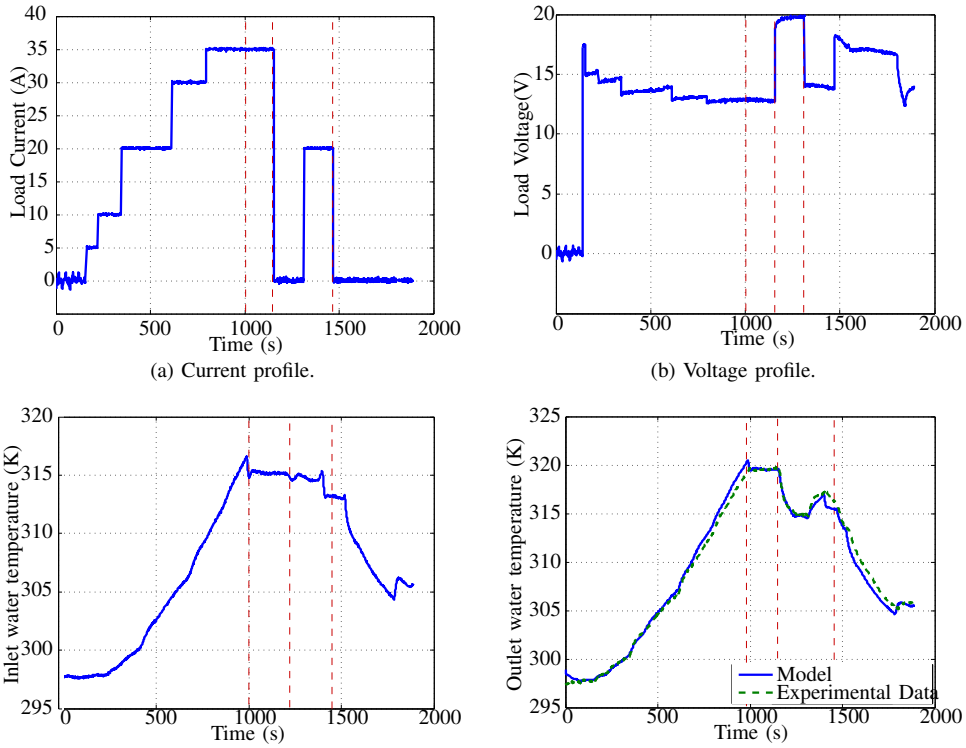

(a) Current profile.

(b) Voltage profile.

(c) Inlet water temperature profile.

(d) Outlet water temperature comparison.

Fig. 7. Validation experiment: startup of the stack.

TABLE II
THERMAL RESISTANCE VALUES.

Parameter	Value (K/W)
R_1	4.2721
R_2	0.2521
R_3	21.0227
R_4	0.3178
R_5	0.3178
R_6	21.0227
R_7	0.2521
R_8	4.2721
R_9	0.3178
$1/(hA)$	0.333

the temperature of the stack, not only in a given operating point, where the parameters where fitted but also in a wide range of operation. Thus, it can be concluded that, despite the model is not quite complex, it can be accurately employed to represent the thermal process of the stack in both steady-state and during transients in a wide operation range. Therefore, the model can be safely used for simulation and control purposes.

The final values of the model parameters are presented in Table II for thermal resistances and in Table III for thermal capacitances. As stated above, the initial parameters were originally set considering nominal values for the stack materials [28] and then adjusted to fit the data for Case 1 of Table I and the transient experiment in Fig. 8.

The spatial and time variation of the model states are presented in Fig. 9, considering the relative position of each section (the first left section is parametrized with relative position 0%, while the last right section is 100%). The

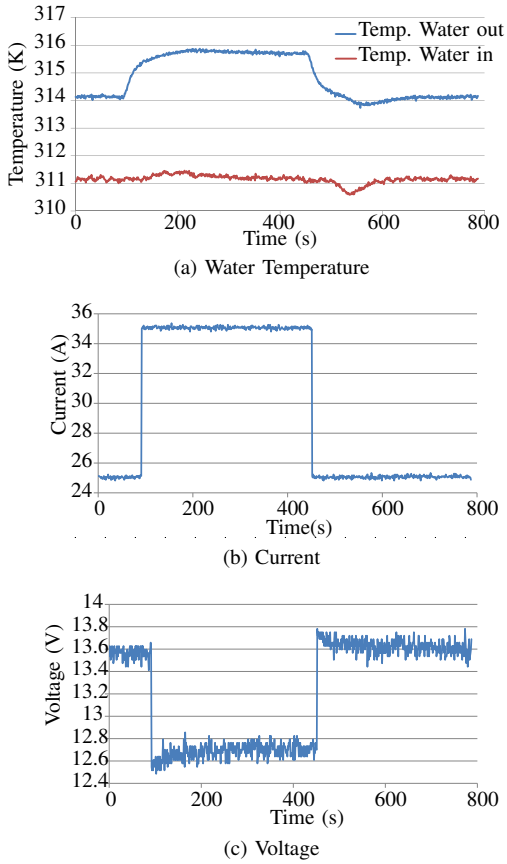

(a) Water Temperature

(b) Current

(c) Voltage

Fig. 8. Experiment to fit the thermal capacitances for the transient state.

TABLE III
THERMAL CAPACITANCE VALUES.

Parameter	Value (J/K)
C_{ai}	255.68
C_{ad}	255.68
C_b	26.9777
C_{bai}	26.9777
C_{cp}	0.2698

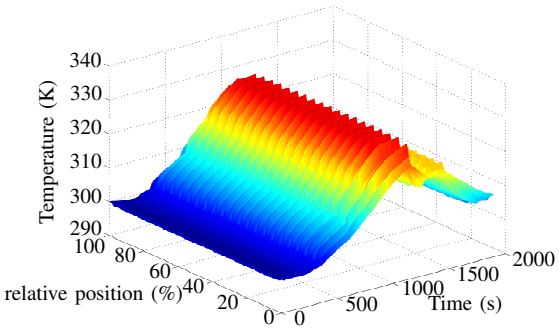

Fig. 9. Spatial variation of temperature across the stack.

peak temperatures are found in the membrane neighbourhoods (where the exothermic reaction takes place) while the lowest temperatures correspond to the cooling water channels, as expected. The temperature between cells is quite similar due to the effect of the distributed water cooling.

The largest temperature difference is found close to the endplates. These components have a significantly larger thermal capacitance and less thermal resistance. In the left side (cell one), the temperature is higher due to the lack of water channels between the endplate and the first cell submodel. The right side (cell 20) has lower temperature, because of the presence of the water channel, and no power generation between the last cell and the endplate.

In Fig. 9, the variation across the stack is represented in a 3D plot for the experiment presented in Fig. 7d. As it can be seen, the effect of the water channels is to homogenise the variation of the temperature along the stack. The space variation is presented as a percentage of the total length of the stack.

C. Simulation example

A simulation example is presented to show the benefits of counting with a model obtained with the proposed methodology. Using the validated parameters of the station, a voltage disturbance in some of the cells was simulated to see the effect on the temperature across the stack. In Fig. 10, the current drawn from the stack is increased at $t = 50$s and the voltage disturbance occurs at $t = 100$ s. As it can be observed, the distribution is no longer symmetric due to the difference in power drawn from certain cells. It is clear than this model is also useful for supervision of the PEM fuel cell stack, in the sense that, using only the knowledge of voltage and current from each cell, it is possible to have an idea of the deviation of the temperatures for each cell.

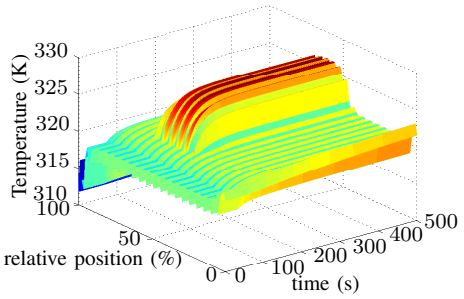

Fig. 10. Simulation of a voltage disturbance in some of the membranes of the stack.

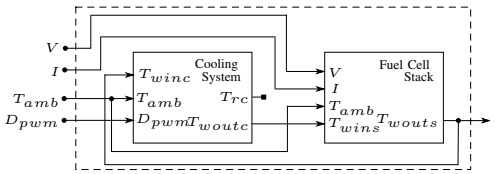

Fig. 11. Block diagram of the thermal model of the station.

D. Thermal modelling of the cooling system

The model obtained for the temperature of the stack is intended to be used for control purposes. Therefore, it is necessary to also model the cooling system in order to have an extended model that includes the thermal management mechanisms. Since the stack modelled in Section II-A is considered to be water-cooled, it is also necessary to model the cooling subsystem used to regulate the stack temperature. The modelling approach of the cooling subsystem is different from the stack thermal model. In this case, a gray-box approach is chosen, where the user computes the model parameters based on physical principles, by means of a mathematical optimisation procedure [30]. The reason behind using this approach is that the analysis of the internal structure of the heat exchanger is not necessary for stack control-oriented modelling.

The considered cooling subsystem consists of a closed-loop pipe where the water is cooled using a heat sink with two fans, as depicted in Fig. 11. In this figure, V is the voltage of the complete stack, I is the drawn current, T_{amb} is the room temperature, D_{pwm} is the duty cycle that commands the fans velocity, T_{rc} is the temperature of the heat exchanger walls, T_{woutc} is the temperature of the output water of the cooling system (which is supposed to be equal to T_{wins}), the input water temperature entering to the stack and T_{winc} is the inlet water temperature to the cooling subsystem (which is also supposed to be equal to T_{wouts}, the outlet water temperature). All inputs are considered as measurable disturbances, except D_{pwm}, which is treated as the system control input. With these considerations, the proposed model for the cooling subsystem is given by

$$\frac{dT_{rc}}{dt} = K_1 D_{pwm} \left(T_{amb} - T_{rc}\right) + K_2 \left(T_{woutc} - T_{rc}\right) + K_3 \left(T_{amb} - T_{rc}\right), \quad (15a)$$

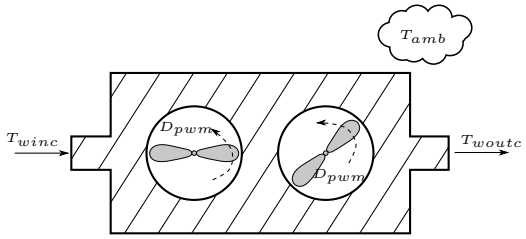

Fig. 12. Diagram of the cooling system

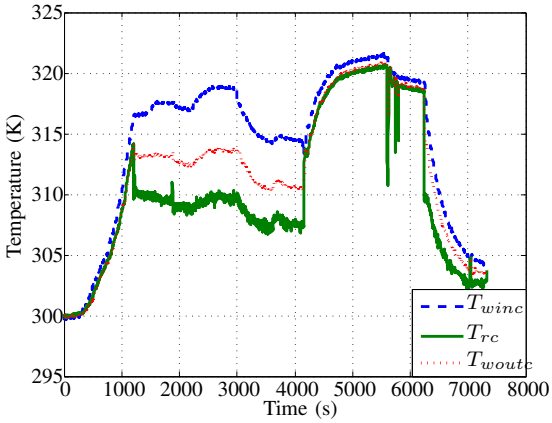

Fig. 13. Data used to calibrate the parameters of the cooling system model.

$$\frac{dT_{woutc}}{dt} = K_4 \left(T_{rc} - T_{woutc}\right) + K_5 \left(T_{winc} - T_{woutc}\right), \tag{15b}$$

where K_i, $i \in \{1, \ldots, 5\}$ are the model parameters to be computed depending on the experimental data. The conceptual diagram of the cooling system is depicted in Fig. 12. The water is cooled by means of the air flow from the fans. In (15), a simple proportional variation is considered. The model of the components correspond to the energy flow due to different gradients of temperatures (between the water and the walls of the heat exchanger, the walls and the air, and between the input and output water temperature).

E. Cooling system model validation

In order to use the model of the cooling system presented in (15), it is necessary to have a set of data available to find the optimal values of the parameters. The data considered for this computation are depicted in Fig. 13. These data were obtained by varying the value of D_{pwm} and measuring the water temperature in the inlet (T_{winc}) and outlet of the cooling system as well as an approximation of the temperature of the cooling walls (T_{rc}). To tune the model parameters, an optimization algorithm for grey-box models included in the System Identification Toolbox in MATLAB was employed. The optimal parameters obtained are $K_1 = 0.1596$, $K_2 = 12.6424$, $K_3 = 0.5884$, $K_4 = 2.4973$, $K_5 = 2.5159$. These parameters determine the velocity of the change in the input variables with respect to the current values of the states. As the case of the PEMFC thermal model, the cooling system model is tested using both steady state and dynamic information. The data used for crossed validation correspond to a different experiment than the data used for the parameter estimation.

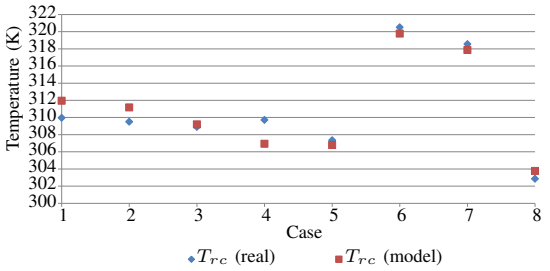

Fig. 14. Validation for T_{rc} in steady state.

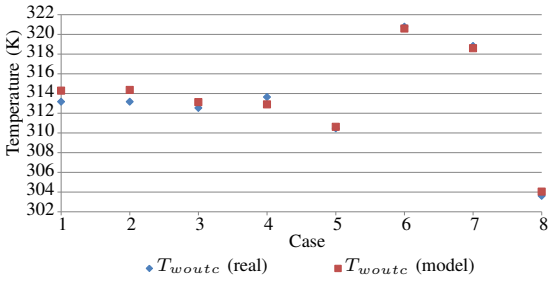

Fig. 15. Validation for T_{woutc} in steady state.

In Table IV, the results of the comparison are presented for different operating points while depicted in Fig. 14 and 15. Using the calibrated model, it is possible to accurately compute the steady state value of the each state variable. However, due to the simple nonlinear approximation of the effect of D_{pwm} over T_{rc} (when $D_{pwm} = 100\%$), the error is almost 3 K (1%). However, for the complete model (stack plus cooling system), the main state to be considered is T_{woutc}, and for all the considered operating points, the maximum error between the model output and the real data was 1.2 K (0.4%).

The cooling system model is also validated for the transient state. The comparison is presented in Fig. 16. As it can be seen, the model is able to efficiently represent the variation in the signal produced by the changes of D_{pwm} and T_{winc}.

IV. Conclusions

In this paper, a control-oriented thermal modelling methodology for PEMFC stacks with water cooling was presented.

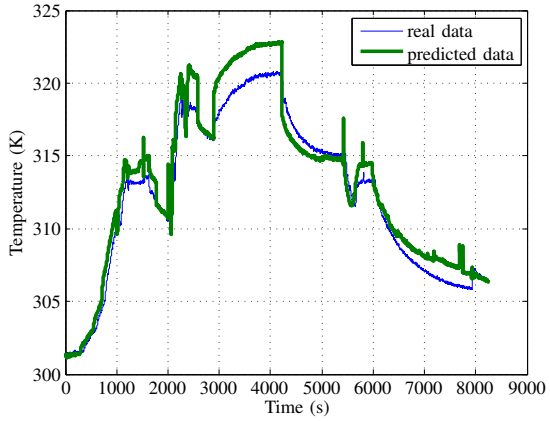

Fig. 16. Dynamical validation of the cooling system model.

TABLE IV
STEADY STATE VALIDATION OF THE COOLING SYSTEM MODEL.

Case	T_{winc} (K)	D_{pwm} (%)	T_{amb} (K)	T_{rc} (K)	T_{woutc} (K)	Model T_{rc} (K)	Model T_{woutc} (K)	T_{rc} difference (K)	T_{woutc} difference (K)
1	316.6	13.8	301.4	310.0	313.2	312.0	314.3	2.0	1.1
2	317.5	23.1	301.8	309.5	313.2	311.2	314.4	1.7	1.2
3	317.0	40.0	302.1	308.9	312.5	309.2	313.1	0.3	0.6
4	318.8	100.0	302.4	309.7	313.6	306.9	312.9	-2.8	-0.7
5	314.4	65.0	302.4	307.3	310.5	306.8	310.6	-0.6	0.1
6	321.4	0.0	302.3	320.5	320.8	319.8	320.6	-0.7	-0.2
7	319.3	0.0	302.4	318.6	318.8	317.9	318.6	-0.7	-0.2
8	304.3	12.9	302.5	302.8	303.6	303.8	304.0	0.9	0.4

This methodology is useful for both monitoring and control purposes. The model can be employed for fuel-cell stacks of any number of cells, since the different components of the model are modular. The validation of the model for both the steady and the transient state was presented using a 600W, 20-cell PEMFC test bench. Also, an empirical non-linear model for the heat exchanger cooling system of the test bench was proposed to be used in conjunction with the thermal model of the stack. The results show that the model approximates the response of the system with high accuracy in a large range of operating points.

REFERENCES

[1] H. Nehrir, C. Wang, and S. Shaw, "Fuel cells: promising devices for distributed generation," *Power and Energy Magazine, IEEE*, vol. 4, no. 1, pp. 47 – 53, 2006.

[2] S.-J. Cheng, Y.-K. Lo, H.-J. Chiu, and S.-W. Kuo, "High-efficiency digital-controlled interleaved power converter for high-power PEM fuel-cell applications," *Industrial Electronics, IEEE Transactions on*, vol. 60, no. 2, pp. 773–780, 2013.

[3] F. Barbir, *PEM Fuel Cells: Theory and Practice*, 1st ed., ser. Sustainable World. Elsevier Academic Press, 2005.

[4] J. Kim, J. Lee, and B. Cho, "Equivalent circuit modeling of PEM fuel cell degradation combined with a LFRC," *Industrial Electronics, IEEE Transactions on*, vol. 60, no. 11, pp. 5086–5094, 2013.

[5] S. Puranik, A. Keyhani, and F. Khorrami, "State-space modeling of proton exchange membrane fuel cell," *Energy Conversion, IEEE Transactions on*, vol. 25, no. 3, pp. 804–813, 2010.

[6] A. Arce, A. del Real, C. Bordons, and D. Ramirez, "Real-time implementation of a constrained MPC for efficient airflow control in a PEM fuel cell," *Industrial Electronics, IEEE Transactions on*, vol. 57, no. 6, pp. 1892–1905, 2010.

[7] S. G. Kandlikar and Z. Lu, "Thermal management issues in a PEMFC stack - A brief review of current status," *Applied Thermal Engineering*, vol. 29, no. 7, pp. 1276 – 1280, 2009, selected Papers from the 10th UK National Heat Transfer Conference, Edinburgh, Scotland, September 10-11, 2007.

[8] Y. Hung, H. Tawfik, D. Mahajan, and M. Zoghi, "Heat transfer analysis of air cooling in forced air and forced convection PEM fuel cells," in *Energy and Sustainability Conference (IESC), 2012 International*, March 2012, pp. 1–8.

[9] X. Yu, B. Zhou, and A. Sobiesiak, "Water and thermal management for Ballard PEM fuel cell stack," *Journal of Power Sources*, vol. 147, no. 1-2, pp. 184 – 195, 2005.

[10] P. Hu, G. Y. Cao, X. J. Zhu, and M. Hu, "Coolant circuit modeling and temperature fuzzy control of proton exchange membrane fuel cells," *International Journal of Hydrogen Energy*, vol. 35, no. 17, pp. 9110 – 9123, 2010.

[11] J. W. Ahn and S. Y. Choe, "Coolant controls of a PEM fuel cell system," *Journal of Power Sources*, vol. 179, no. 1, pp. 252 – 264, 2008.

[12] G. Vasu and A. Tangirala, "Control-orientated thermal model for proton-exchange membrane fuel cell systems," *Journal of Power Sources*, vol. 183, no. 1, pp. 98 – 108, 2008.

[13] J. T. Pukrushpan, "Modeling and control of fuel cell systems and fuel processors," Ph.D. dissertation, The University of Michigan, 2003.

[14] A. J. del Real, A. Arce, and C. Bordons, "Development and experimental validation of a PEM fuel cell dynamic model," *Journal of Power Sources*, vol. 173, no. 1, pp. 310 – 324, 2007.

[15] F. Gao, B. Blunier, M. Simoes, and A. Miraoui, "PEM fuel cell stack modeling for real-time emulation in hardware-in-the-loop applications," *Energy Conversion, IEEE Transactions on*, vol. 26, no. 1, pp. 184–194, March 2011.

[16] A. Salah, J. Gaber, R. Outbib, O. Serres, and H. El-Sayed, "Modeling and Simulation of PEM Fuel Cell Thermal Behavior on Parallel Computers," *Energy Conversion, IEEE Transactions on*, vol. 25, no. 3, pp. 768 –777, 2010.

[17] K. C. Lauzze and D. J. Chmielewski, "Power control of a polymer electrolyte membrane fuel cell," *Industrial & Engineering Chemistry Research*, vol. 45, no. 13, pp. 4661–4670, 2006.

[18] F. Gao, B. Blunier, A. Miraoui, and A. El-Moudni, "A multiphysic dynamic 1-D model of a proton-exchange-membrane fuel-cell stack for real-time simulation," *Industrial Electronics, IEEE Transactions on*, vol. 57, no. 6, pp. 1853–1864, 2010.

[19] L. Gauchia and J. Sanz, "A per-unit hardware-in-the-loop simulation of a fuel cell/battery hybrid energy system," *Industrial Electronics, IEEE Transactions on*, vol. 57, no. 4, pp. 1186–1194, 2010.

[20] J.-H. Jung, S. Ahmed, and P. Enjeti, "PEM fuel cell stack model development for real-time simulation applications," *Industrial Electronics, IEEE Transactions on*, vol. 58, no. 9, pp. 4217–4231, 2011.

[21] L. Dumercy, R. Glises, J. Kauffmann, and H. Louahlia-Galous, "Transient thermal computation of a PEM fuel cell by a nodal modeling," in *Vehicular Technology Conference, 2003. VTC 2003-Fall. 2003 IEEE 58th*, vol. 5, October 2003, pp. 3299 – 3303 Vol.5.

[22] Y. Qun, L. Qing, Z. Peichang, and Y. Datai, "Temperature modeling of PEM fuel cell based on fuzzy strategy," in *Control and Decision Conference (2014 CCDC), The 26th Chinese*, May 2014, pp. 2383–2387.

[23] X. Kong and A. Khambadkone, "Modeling of a PEM fuel-cell stack for dynamic and steady-state operation using ANN-based submodels," *Industrial Electronics, IEEE Transactions on*, vol. 56, no. 12, pp. 4903–4914, 2009.

[24] J. Rojas, C. Ocampo-Martinez, and C. Kunusch, "Thermal modelling approach and model predictive control of a water-cooled PEM fuel cell system," in *Industrial Electronics Society, IECON 2013 - 39th Annual Conference of the IEEE*, Nov 2013, pp. 3806–3811.

[25] J. Hwang, D. Wang, and N. Shih, "Development of a lightweight fuel cell vehicle," *Journal of Power Sources*, vol. 141, no. 1, pp. 108 – 115, 2005.

[26] J. Moré, P. Puleston, C. Kunusch, and A. Visintin, "Temperature control of a PEM fuel cell test bench for experimental MEA assessment," *International Journal of Hydrogen Energy*, vol. 35, no. 11, pp. 5985 – 5990, 2010.

[27] C. J. Geankoplis, *Procesos de Transporte y Operaciones Unitarias*, 3rd ed. Compañía Editorial Continental, S.A. DE C.V. México, 1998.

[28] J. J. Moré, "Automatización de Sistemas de Celdas de Combustible tipo PEM," Master's thesis, Facultad de Ingeniería, Universidad Nacional de la Plata, 2007.

[29] M. Gilli, D. Maringer, and E. Schumann, "Chapter twelve - heuristic methods in a nutshell," in *Numerical Methods and Optimization in Finance*, M. G. M. Schumann, Ed. San Diego: Academic Press, 2011, pp. 337 – 379.

[30] B. Sohlberg, "Grey box modelling for model predictive control of a heating process," *Journal of Process Control*, vol. 13, no. 3, pp. 225 – 238, 2003.